remote sensing

MDPI

Article

Monitoring Land-Use/Land-Cover Changes at a Provincial Large Scale Using an Object-Oriented Technique and Medium-Resolution Remote-Sensing Images

Kaisheng Luo [1,*], Bingjuan Li [2,3] and Juana P. Moiwo [4]

1 School of Remote Sensing and Geomatics Engineering, Nanjing University of Information Science and Technology, Nanjing 210044, China
2 Institute of Soil Science, Chinese Academy of Sciences, Nanjing 210008, China; bjli@issas.ac.cn
3 University of Chinese Academy of Sciences, Nanjing 210008, China
4 Department of Agricultural Engineering, School of Technology, Njala University, Freetown, Sierra Leone; jupamo2001@yahoo.com
* Correspondence: 002872@nuist.edu.cn; Tel.: +86-188-6095-7185

Received: 30 October 2018; Accepted: 8 December 2018; Published: 12 December 2018

Abstract: An object-based image analysis (OBIA) technique is replacing traditional pixel-based methods and setting a new standard for monitoring land-use/land-cover changes (LUCC). To date, however, studies have focused mainly on small-scale exploratory experiments and high-resolution remote-sensing images. Therefore, this study used OBIA techniques and medium-resolution Chinese HJ-CCD images to monitor LUCC at the provincial scale. The results showed that while woodland was mainly distributed in the west, south, and east mountain areas of Hunan Province, the west had the largest area and most continuous distribution. Wetland was distributed mainly in the northern plain area, and cultivated land was distributed mainly in the central and northern plains and mountain valleys. The largest impervious surface was the Changzhutan urban agglomerate in the northeast plain area. The spatial distribution of land cover in Hunan Province was closely related to topography, government policy, and economic development. For the period 2000–2010, the areas of cultivated land transformed into woodland, grassland, and wetland were 183.87 km^2, 5.57 km^2, and 70.02 km^2, respectively, indicating that the government-promoted ecologically engineered construction was yielding some results. The rapid economic growth and urbanization, high resource development intensity, and other natural factors offset the gains made in ecologically engineered construction and in increasing forest and wetland areas, respectively, by 229.82 km^2 and 132.12 km^2 from 2000 to 2010 in Hunan Province. The results also showed large spatial differences in change amplitude (LUCCA), change speed (LUCCS), and transformation processes in Hunan Province. The Changzhutan urban agglomerate and the surrounding prefectures had the largest LUCCA and LUCCS, where the dominant land cover accounted for the conversion of some 189.76 km^2 of cultivated land, 129.30 km^2 of woodland, and 6.12 km^2 of wetland into impervious surfaces in 2000–2010. This conversion was attributed to accelerated urbanization and rapid economic growth in this region.

Keywords: HJ-CCD images; object-based image analysis; change monitoring; provincial scale

1. Introduction

Land-use/land-cover change (LUCC) is one of the most direct signals used to determine the impact of anthropogenic activity on the ecosystem, and it also provides the link between human

socioeconomic activities and natural ecological processes [1,2]. This process is closely related to the processes of terrestrial surface material cycle and life and has a direct impact on the biosphere, atmosphere interaction, biological diversity, surface radiation force, biogeochemical cycle, and the sustainable utilization of resources and the environment [3–5]. Therefore, LUCC has become the focus of research on global climate and environmental change [6,7].

Remote-sensing technology has developed rapidly because of its macroscopic, rapid, and abundant information capture ability, and it is widely used in the dynamic monitoring of LUCC [8]. Technically, LUCC monitoring methods based on remote sensing are divided into a traditional pixel-based method and an object-based image analysis (OBIA) method [9]. Remote-sensing monitored change is accomplished by (1) LUCC classification and comparison of classified results; and (2) LUCC detection and classification of detected change [10]. The traditional pixel-based method fully excavates and uses spectral features of images, exploring a series of algorithms, which include the maximum likelihood, minimum distance, Markova distance, parallel hexahedron, K-neighbor, K-mean value, iterative self-organizing data analysis, and newly emerging support vector machines algorithms. Breakthroughs are difficult to achieve, however, in monitoring accuracy using the traditional pixel-based method and determining the level of noise because of high spectral similarity. The traditional pixel-based method mainly uses spectral information, other than a portion of texture information, and cannot fully mine the shape, spatial position, and spatial structure of remote-sensing data. In many cases, more information than pixels can be obtained only when the image is segmented into homogeneous objects, which can further improve the monitoring accuracy [11,12].

The OBIA technique is based on the smallest processing unit object (i.e., a set of adjacent homogeneous pixels), which has revolutionized the traditional pixel-based method [8]. The OBIA technique not only uses spectral features of ground objects but also makes full use of spatial features, texture, spatial structures, shape, and other characteristics during monitoring of LUCC. To a large extent, it overcomes the "salt and pepper" effect caused by spectral similarity and image noise and also improves monitoring accuracy [12]. According to the literature, land cover monitoring accuracy from the OBIA technique is higher than that from the traditional pixel-based method, and boundary conditions are more consistent with ground conditions [13–15]. The OBIA technique is replacing traditional pixel-based LUCC monitoring and is becoming the new standard [16–20].

Previous research on OBIA mainly focused on high-resolution remote-sensing images, such as WorldView-2, QuickBird, GeoEye-1, and IKONOS images [18]. By using the OBIA technique, high-resolution images can be used to monitor LUCC daily because of their abundant information. Due to the high price of high-resolution images, however, the research area has to be relatively small, mostly exploratory, and small scale in nature, which limits the large-scale application of the OBIA technique. LUCC is a global issue that requires the large-scale study and monitoring of dynamic LUCC [21,22]. It is almost impossible to monitor dynamic LUCC at the regional scale using high-resolution remote-sensing images because of the high costs. Additionally, low-resolution images are too rough to ensure high accuracy. Thus, using medium-resolution remote-sensing images is the best available choice. Object-oriented LUCC change monitoring using medium-resolution remote-sensing images is scarce. How can we use OBIA technology for the large-scale monitoring of LUCC based on medium-resolution remote-sensing images? What are the feasible processes and methods? How effective is the use of the OBIA technique and medium-resolution remote-sensing images for large-scale LUCC monitoring? To answer these questions, it is necessary to apply the OBIA technique to a medium-resolution remote-sensing image (such as HJ-CCD image or Landsat TM) to verify OBIA performance and results in the large-scale monitoring of LUCC.

A province is an administrative area in China that is fairly large and therefore can represent a large-scale area. LUCC monitoring at the provincial scale is an important requirement for the implementation of specific measures at the provincial level. Dynamic LUCC information is quite important for policymakers, because this information is often urgently needed for given periods

and spatial expanses, including changes in quantity and spatial patterns, to formulate policy measures [23,24].

On the basis of this need, we used China's medium-resolution HJ-CCD image and the OBIA technique to monitor dynamic LUCC information in Hunan Province for the period 2000–2010. The aim of the study was to clarify spatiotemporal changes in LUCC for the period 2000–2010, analyze the LUCC transformation process, and further discusses the internal mechanisms of LUCC in the study area.

2. Materials

2.1. Study Area

The study area is Hunan Province, one of the 34 provinces in China. Hunan Province lies in the south of the middle reaches of Yangtze River, north of Nanling Mountains, between 39°24′–30°08′N and 108°47′–114°15′E. The land area of the province is 211,800 km^2, with rich and diverse land resources, mountains, hills, and plains accounting for 56%, 24%, and 20% of the area, respectively. Hunan Province is in the transition zone of the second and third steppes in China with an altitude of 3–1925 m. The terrain is surrounded largely by mountains in the east, west, and south, with a plain in the middle and land that is slightly open to the north. The climate belongs to the subtropical monsoon climate zone, with an average temperature of 15–17 °C (maximum of 39 °C and minimum of 3.2 °C) and annual rainfall of 800–1600 mm. The main soil types include red soil, yellow soil, yellow-brown soil, and dark-brown soil [25]. Hunan Province has a population of 7.32 × 10^7 people and ranks seventh among Chinese provinces. The gross domestic product (GDP) of Hunan Province in 2017 was 4.46 × 10^{12} RMB, ranking ninth among all of the provinces in China. Hunan is a large agricultural province, in which the yield of rice is the largest in the country. Hunan Province consists of 14 prefectures, with strong human activities, and complex and broken landscapes (Figure 1).

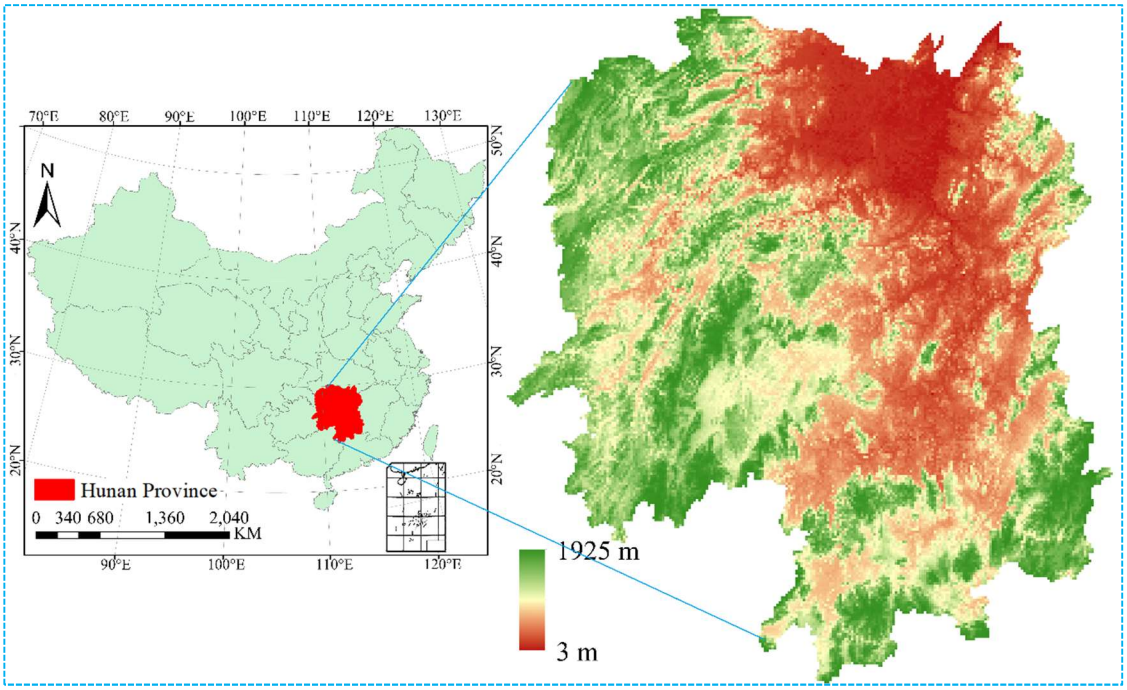

Figure 1. Location of Hunan Province in China (red spot in plate on the left) and an expanded version of the province (plate on the right) depicting land surface elevation.

From 2000 to 2010, Hunan Province in China was strongly affected by intensive anthropogenic activity, characterized by rapid economic growth and accelerated urbanization with a significant impact on LUCC [26,27]. To improve the ecological environment and protect woodlands, grasslands,

and wetlands in the region, the government successively carried out major ecological projects, including "Returning Farmland to Woodland or Grassland", "Natural Forest Protection" and "Returning Farmland to Lake" [26,27]. Under such conditions, questions have been raised about the effectiveness of these ecological projects and about the changes that have taken place in LUCC in Hunan Province under the effect of climate change and human activities. Answers are needed urgently, and therefore, the selection of Hunan Province as a research area has typical and important reference value.

2.2. Satellite Imagery

In this study, we used China's HJ-CCD satellite image Landsat TM as the main remote-sensing data source. We used the HJ-CCD image to map land use information for 2010 and used the Landsat TM image for reconstruction land use information for 2000. Because Landsat TM and HJ-CCD images have the same bands (including red band, green band, blue band, and near infrared band), spatial resolution and similar image features, we used both images to detect changes that occurred between 2000 and 2010. HJ satellites, including the A satellite and B satellite, were launched successfully in September 2008. The satellites are equipped with CCD cameras of four bands with a spatial resolution of 30 m and a revisit period (temporal resolution) of 2–3 days. The main parameters of the HJ-CCD images are shown in Table 1 [28]. Considering the obvious seasonal changes of vegetation and the need for improved classification, we used HJ-CCD images for spring, summer, and winter. To avoid the effect of cloudy weather in southern China on the image quality, we selected 30 clear images, including 12 scenes in spring, 10 scenes in summer, and 8 scenes in winter. In the 30 image scenes, 14 were from the A satellite (HJA-CCD) and 16 were from the B satellite (HJB-CCD) (Table S1). The HJ-CCD images were downloaded from the China Centre for Resources Satellite Data and Application at http://www.cresda.com/CN/. The experimental images included 24 scenes of Landsat TM images for 2000, which come from the Geospatial Data Cloud of China (http://www.gscloud.cn/).

Table 1. List of the main parameters of China's HJ-CCD image.

Spectral Band	Spatial Resolution	Spectral Range
Band 1: blue	30 m	0.43–0.52 μm
Band 2: green	30 m	0.52–0.60 μm
Band 3: red	30 m	0.63–0.69 μm
Band 4: near infrared	30 m	0.76–0.90 μm

2.3. Field Data

We conducted field sampling in 2010 and used the collected field data to verify the results of the classified land uses in the study area (Figure 2). We conducted the field sampling three times across Hubei province: in spring (March), summer (June), and winter (December), with each period lasting for one month. In this study, we used stratified random sampling to collect field samples. In the field sampling route design, we considered image characteristics and traffic accessibility. The whole field sampling work is based basically on the random sampling of ground objects within a 2-km range along the road. According to the area ratio based on historical data, a number of field samples for each land cover type is obtained. In addition, to maintain a uniform distribution of samples in each region, we guaranteed that the route of each sample was different. On the basis of the complexity and dispersity of environmental elements, the complex environment needed additional sample points, so the distribution of samples was denser in areas with complex and fragmented landscapes. During field sampling, we first used handheld GPS devices to locate the latitude and longitude of the sample scene, and then we measured the various attributes of the scene, including land cover type, tree species, and slope degree of the area. We collected a total of 1644 field samples, with 158 samples in spring, 347 samples in summer, and 1139 samples in winter.

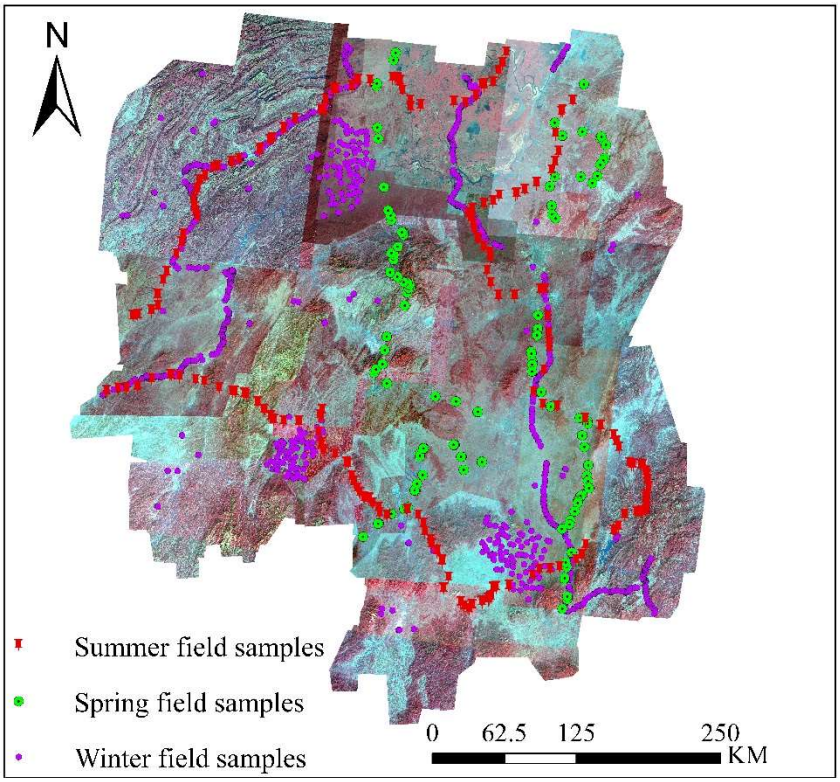

Figure 2. Field sample and sampling route in spring, summer, and winter.

2.4. Reference Data

Auxiliary data mainly included a digital elevation model (DEM), slope degree map, Landsat TM images, Google Earth images, and a boundary vector map of Hunan Province. DEM data with a 30 m resolution came from the Geospatial Data Cloud of China (http://www.gscloud.cn/). The slope map was generated in ERDAS 9.2 software using the DEM. The boundary vector map of Hunan Province came from the China Resources and Environment Data Cloud Platform (http://www.resdc.cn/). We used the Landsat TM images as the reference images for geometric correction of the HJ-CCD images.

3. Methods

In this study, we first pre-processed the HJ-CCD images and other spatial data and classified the 2010 land cover using OBIA. Next, we detected changes using the 2000 Landsat TM and 2010 HJ-CCD images to identify areas that experienced change. After that, we transformed the land use results for 2010 into samples with a corresponding category and classified the area of change for 2000 according to the most adjacent OBIA classifier. We updated the classification results of the area of change in 2000 to the land cover map for 2010 to reconstruct the 2000 land cover map for Hunan Province. We superimposed the land cover maps for 2000 and 2010 to obtain land cover changes that occurred in Hunan Province between 2000 and 2010. A detailed flowchart of the research process is given in Figure 3.

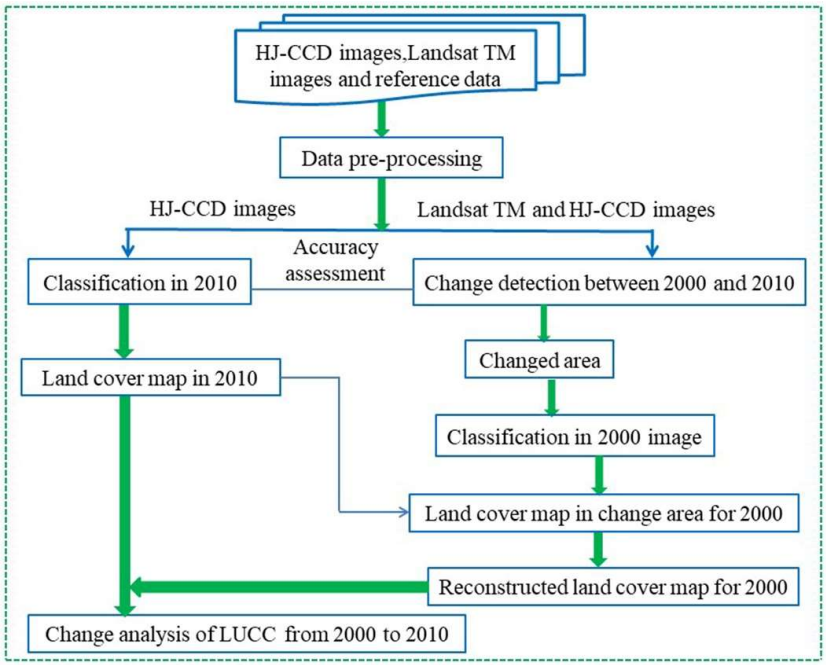

Figure 3. A flowchart of the classification process used to assess land-use/land-cover changes (LUCC) in Hunan Province study area.

3.1. Data Preprocessing

The data preprocessing mainly included projection, transformation, mosaicking, clipping, geometric correction, atmospheric correction, and image segmentation. We used the WGS84 coordinate system and UTM projection for the spatial data. Since Landsat TM images from the Geospatial Data Cloud of China (http://www.gscloud.cn/) have been geometrically refined, we used the Landsat TM images as reference data. Specially, we randomly selected the corresponding position point in Landsat TM as the ground control points, and then we used quadratic polynomial transformation and bilinear interpolation to carry out geometric correction. To ensure the accuracy of geometric correction, we controlled the root mean squared error value at around 0.5. We corrected the geometric precision of the HJ-CCD images using the geometric correction module of ERDAS 9.2 software. Since the HJ-A/B satellites have 360 km coverage, a small sub-satellite error point, and a large surrounding deformation, the HJ-CCD images for the mountain areas needed additional ortho-rectification using DEM. Using the calibration parameters provided by the China Resources Satellite Application Center, we successfully calibrated all of the images [29]. Considering the processing power of the computer and the characteristics of the underlying surface, we divided and coded the pre-processed HJ-CCD data for Hunan Province into 28 small images. On the basis of the latitude and longitude coordinates, we input the field samples into ArcGIS to convert the samples into a point vector map and then converted the collected attributes of the sample data into corresponding auxiliary data. We obtained the data for the research area by clipping along the administrative boundary of Hunan Province.

3.2. Object-Based Image Analysis Technique

The OBIA used in this study was based on the smallest unit: in this case, an object with physical meaning, which is a set of adjacent pixels with homogeneity [17]. The basic process of OBIA includes image segmentation and then classification or change detection.

3.2.1. Image Segmentation

In this study, we used a region-merging algorithm that is based on the principle of least heterogeneity to segment images. The basic concept of this algorithm is to assemble adjacent pixels

with similarity into polygons. This method first identifies a seed pixel in an area of interest and then splits this pixel as a starting point in the growth. Then, the seed pixel is merged to an adjacent pixel with homogeneity. Next, the new pixels are used as a new seed to repeat this process, until no pixel meets the defined conditions [18], which terminates the segmentation scale [17]. The larger the segmentation scale, the smaller the number of objects obtained and vice versa. Because of the difference in land features, structures, and landscape fragmentation, the appropriate segmentation scale for each type of land cover in the different study areas was different [22]. When the segmentation scale is too large, small grounds are likely to be submerged and to become non-extractable. If the segmentation scale is too small, the computer becomes burdened and produces results with high "salt and pepper" noise [17]. The trial-and-error method is widely used to determine the appropriate segmentation scale. Through repeated attempts, we determined the appropriate segmentation scale for each small section of the image of Hunan Province (Table S2).

3.2.2. 2010 Land Cover Classification

This research adopted the land cover classification system of the Intergovernmental Panel on Climate Change (IPCC). Land cover included woodland, grassland, wetland, farmland, impervious surface, and bare land. In this study, we used a binary decision tree to classify land cover in Hunan Province for 2010 (Figure 4). First, we divided the images into wetland and non-wetland using the near infrared band of HJ-CCD images in the summer. Then, we divided the non-wetland normalized difference vegetation index (NDVI) into vegetation and non-vegetation areas. The farmland slope in Hunan Province is no more than 25° and the soil-adjusted vegetation index (SAVI) can eliminate the effect of soil on the NDVI index (Table 2). Therefore, we divided the vegetation into farmland and non-farmland using SAVI and slope indicators of the summer images. We again divided the non-farmland into woodland and non-woodland (grassland in the study area) based on differences in biomass. We used NDVI to characterize the biomass, but it was difficult to distinguish two categories based only on the biomass in a single season. To widen the distinction, we used cumulative NDVI (ACNDVI) or the sum of three seasons to measure the annual biomass. At the same time, we found that while the distribution of woodland in the study area was closely related to elevation, the texture of grassland in the HJ-CCD image was much rougher than that of woodland. Therefore, we made comprehensive use of ACNDVI, DEM, and texture indicators to distinguish woodland from grassland. The degrees of brightness of impervious surface and bare land were different, and the impervious surface object in the HJ-CCD image was more compact than the bare land. Thus, we comprehensively used brightness and compactness to distinguish these two attributes.

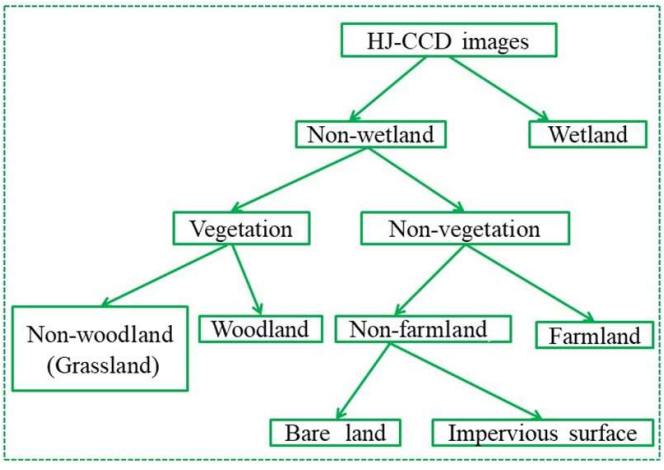

Figure 4. Binary decision tree used to process the remote-sensing images for the Hunan Province study area.

Table 2. Extraction features of the binary decision tree used to process the remote-sensing images for the Hunan Province study area. NDVI: normalized difference vegetation index; SAVI: soil-adjusted vegetation index; ACNDVI: cumulative NDVI; DEM: digital elevation model.

Land Cover	Index	Threshold	Note
Wetland	Band 4s	Band 4s $\leq$ 1350~1403	Band 4s are the fourth band of HJ-CCD in summer
Non-wetland	Band 4s	Band 4s > 1350~1403	Same as above
Vegetation	NDVIs	NDVIs $\geq$ 0.32~0.42	NDVI is the NDVI value of HJ-CCD in summer
Non-vegetation	NDVIs	NDVIs < 0.32~0.42	Same as above
Farmland	SAVIs and slope	SAVIs $\leq$ 0.76~0.83 and Slope $\leq$ 22°~27°	SAVIs is the SAVI value of HJ-CCD in summer
Non-farmland	SAVIs and slope	SAVIs > 0.76~0.83 or Slope > 22°~27°	Same as above
Woodland	ACNDVI, DEM and texture (GCLM-A)	ACNDVI $\geq$ 1.38~1.43 and DEM $\geq$ 600 m and 0.21~0.31 $\leq$ GCLM-A $\leq$ 0.35~0.41	ACNDVI is the sum of NDVI in spring, summer and winter, GCLM-A is gray-level co-occurrence matrix for all directions
Non-woodland (grassland)	ACNDVI, DEM and texture (GCLM-A)	ACNDVI < 1.38~1.43 or DEM< 600 m or GCLM-A < 0.21~0.31 or GCLM-A > 0.35~0.41	Same as above
Impervious surface	Brightness and compactness	Brightness $\geq$ 960~1500 and compactness $\geq$ 0.27~0.32	
Bare land	Brightness and compactness	Brightness $\geq$ 960~1500 or compactness $\geq$ 0.27~0.32	

3.2.3. Land Cover Change Detection

We used the vector similarity function of OBIA to detect the changes in HJ-CCD images in 2010 and 2000 and obtained the area of change from differences in the object characteristics for the different periods. We took the image of the base period T_1 and the image of the change period T_2 as an n-dimensional feature vector, and each band/feature as the dimension [30]. The segmentation object of the image in the T_1 period is represented by vector X, where X_n is the nth feature value of any segmented object in the image. Similarly, any object on the image in the T_2 period is represented by vector y, where y_n is the value of the nth feature value of any segmented object in the remote-sensing image. From the principle of vector similarity, the smaller the angle between vectors and the closer the magnitude is, the more similar the two vectors are [30].

$$\mathrm{x} = \begin{bmatrix} x_1 \\ x_2 \\ x_3 \\ . \\ . \\ x_n \end{bmatrix} \mathrm{y} = \begin{bmatrix} y_1 \\ y_2 \\ y_3 \\ . \\ . \\ y_n \end{bmatrix}. \quad (1)$$

The vector similarity function is constructed to measure the similarity. The functions are as follows:

$$f(xy) = \frac{\cos\theta}{||x| - |y||}. \quad (2)$$

To limit the range of change, the following formula is obtained after normalization treatment of Equation (1):

$$f(xy) = \frac{\cos\theta}{\cos\theta + ||x| - |y||} \quad (3)$$

where $f(xy)$ is vector similarity; $|x|$ and $|y|$ are the eigenvectors of the objects in the base period and the change period, respectively; and θ is the angle between eigenvectors for two period. The function $f(xy)$ has a range of 0–1. The smaller $f(xy)$ is, the less similar the image object is; the greater the difference, the more likely the object is to change.

3.3. Land Cover Map Reconstruction for 2000

After obtaining the change area, we automatically classified the area using the nearest neighbor classifier of OBIA. Then, we updated the resulting map of regional classification of change in 2000 to the land cover classification map for 2010 in ArcGIS. We then used this map to reconstruct the land cover map of Hunan Province for 2000. We used the nearest neighbor classifier of OBIA to identify the closest samples for each object based on distance and assigned the objects to a category. This distance was the characteristic parallel distance or Mahalanobis distance. The feature of the nearest neighbor classifier is shown as Table 2.

3.4. Accuracy Verification

We used the confusion matrix method (Table 3) to evaluate the accuracy of the results of the land cover classification for 2010 against the field samples. The extraction of change area was similar to the classification of the remote-sensing images and the difference was the two classes across the image: changed class and unchanged class. We used the overall accuracy (OA) and Kappa coefficient to quantify the accuracy of the result [14,31]. The higher the OA and Kappa values (KV), the higher the accuracy of the results.

$$OA = \sum_{i=1}^{n} p_{ii}/N \quad (4)$$

$$KV = \frac{N\sum_{i=1}^{r} x_{ii} - \sum_{i=1}^{r}(x_{i+} + x_{+i})}{N^2 - \sum_{i=1}^{r}(x_i + x_{+i})} \quad (5)$$

where r is the total number of columns (total number of categories) of the confusion matrix, x_{ii} is the number of objects on the ith row and ith column in the error matrix (number of correct classifications), x_{i+} and x_{+i} are the number of the ith row and ith column, respectively, and N is the total number of field samples used for accuracy evaluation.

Table 3. Confusion matrix.

Measured Data Type	Classification Data Type					Sum of Measured Data
	1	**2**	...	...	***n***	
1	p_{11}	p_{21}	...	...	p_{n1}	p_{+1}
2	p_{12}	p_{22}	...	...	p_{n2}	p_{+2}
...	...		...	...	...	...
...	...		...	...	...	...
n	p_{1n}	p_{2n}	...	...	p_{nn}	p_{+n}
Sum of classification	p_{1+}	p_{2+}	...	...	p_{n+}	N

3.5. Speed and Amplitude of Land Cover Change

We further quantified the LUCC using the indices of LUCC amplitude (LUCCA) and change speed (LUCCS). The calculation formulas of LUCCA and LUCCS are shown in Equations (6) and (7) [32]:

$$S = \left\{ \frac{\sum_{ij}^{n} |\Delta s_{ij}|}{S_i} \right\} \times 100\% \quad (6)$$

$$S = \left\{ \frac{\sum_{ij}^{n} |\Delta s_{ij}|}{TS_i} \right\} \times 100\% \quad (7)$$

where S_i is the percentage of the ith class of land cover in the total study area at the initial stage; ΔS_{ij} is the sum of the area of class i converted into other classes from the beginning to the end of the study period; and T is the length of the period (if expressed in years, then the number is years).

4. Results

4.1. Classification Results and Accuracy

As in Figure 5, the classification map for 2010 and the reconstructed one for 2000 using OBIA were relatively smooth and compact and apparently not broken. Therefore, the map maintained a high distribution consistency with the actual ground conditions. The differences among the different categories were obvious and the boundary shapes of the different categories were relatively clear, which was consistent with the distribution of terrain in the study area (Figures 1 and 5).

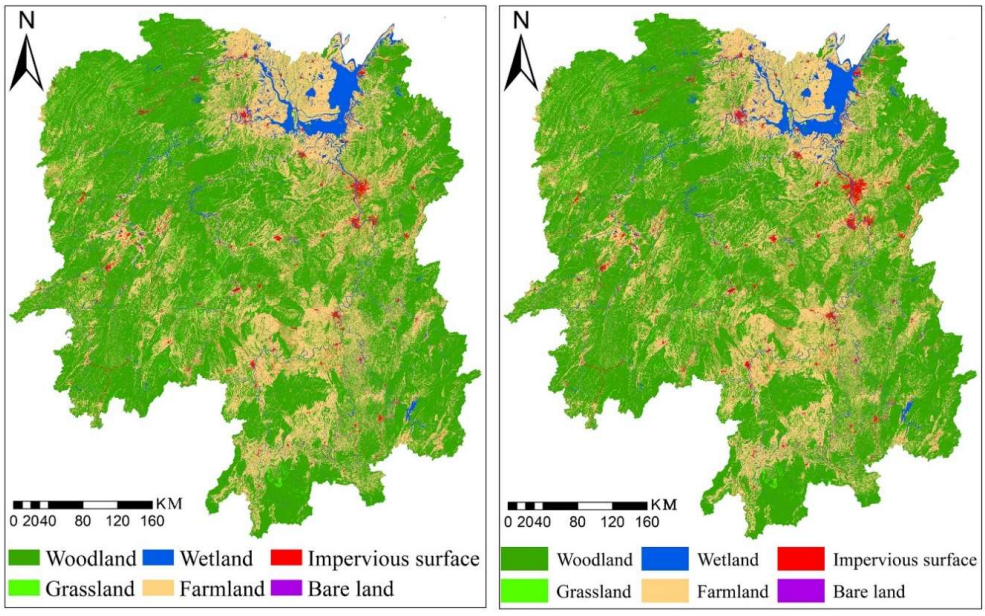

(**a**) (**b**)

Figure 5. Reconstructed land cover map for 2000 (**a**) and the classification results of land cover for 2010 (**b**) for Hunan Province study area.

We evaluated the accuracy of the land cover classification results for 2010 using 1644 field samples. For 2010, the overall accuracy of the land cover classification results for Hunan Province was 93.10% with a Kappa coefficient of 0.89. We evaluated the accuracy of the change detection using 200 sample points. The overall accuracy and the Kappa coefficient of the detected changes were 86.42% and 84.32%, respectively. This showed that the accuracy of the results was high and fully met both research and practical needs.

In 2010, the area of woodland was largest (133,103.62 km^2), accounting for 62.49% of Hunan Province. The next largest was the farmland area (63,572.75 km^2), accounting for 29.86% of the total area of the province. The next largest was the wetland, which covered some 7891.48 km^2, accounting for 3.71% of the total area of the province. The impervious surface was relatively large, with an area of 5308.29 km^2, accounting for 2.49% of the total area of the province. Grassland and bare land had the smallest areas, with 2578.32 km^2 (1.21%) and 516.09 km^2 (0.24%), respectively, of Hunan Province. In 2000, the areas of woodland, farmland, wetland, impervious surface, grassland, and bare land were, respectively, 133,285.08 km^2 (62.60%), 63,995.79 km^2 (30.06%), 7976.29 km^2 (3.75%), 4634.09 km^2 (30.06%), 2570.68 km^2 (1.21%), and 460.77 km^2 (0.22%).

4.2. Land Cover Pattern in Hunan Province

Woodland in Hunan Province was distributed mainly in the mountain areas in the west, south, and east, and the distribution was continuous. Wetlands were concentrated in the northern plains of Hunan Province, with other wetland areas relatively scattered and small. Farmland was distributed widely in the study area but was mainly in the central and northern plains of the province and the valleys in mountain areas. Impervious surfaces were scattered with relatively small patches. The largest area was the Changzhutan urban agglomerate in the northeast plains. The areas of grassland and bare land were among the smallest areas and were scattered throughout the study area.

4.3. Land Cover Change in 2000–2010

4.3.1. Change Characteristics

From 2000 to 2010, the trends in woodland, wetland, and farmland decreased, whereas those in impervious surface, grassland, and bare land increased. The variation of impervious surface in Hunan Province was the largest, increasing by 674.20 km^2. The next largest was farmland, which fell by 423.05 km^2 in 2000–2010. The third largest was woodland, falling by 229.82 km^2 in 2000–2010. Wetland shrank by 84.80 km^2 and grassland experienced the smallest change, increasing by 7.62 km^2.

The LUCCA and LUCCS of LUCC in Hunan Province for 2000–2010 were 1.30% and 0.12%, respectively. Although LUCCA and LUCCS in the whole study area were not very large, large differences existed among the different types of land use/cover. The LUCCA and LUCCS of the bare land were highest, at 19.28% and 1.75%, respectively. The second highest was the impervious surface, with a LUCCA of 15.16% and LUCCS of 1.38%. The third highest was wetland, with a LUCCA of 2.85% and LUCCS of 0.26%. Because of the wide area and large base, the LUCCA and LUCCS of woodland were relatively small at 0.53% and 0.05%, respectively.

4.3.2. Transfer Process

As shown in Table 4, although 183.87 km^2 of farmland was converted into woodland, 200.98 km^2 of woodland was converted into farmland. Thus, the direction of the net conversion after being offset by the conversion of other directions of the study period was from woodland into farmland. Additionally, 214.39 km^2 of woodland was converted into impervious surfaces, significantly reducing woodland area and rapidly increasing impervious surfaces. Although 70.02 km^2 of farmland was converted into wetland, a large portion of wetland was converted into farmland, woodland, and impervious surface, resulting in a net decrease of 132.12 km^2 in wetland. Along with increasing urbanization, industrialization, and economic development, the area of impervious surface rapidly expanded. This increase in impervious surface occurred separately from other land cover types in the study area, among which was the conversion of 445.74 km^2 of farmland (the largest).

As shown in Figure 6a, the distribution pattern of LUCC for 2000–2010 in Hunan Province was greater in the western region than in the eastern region, greater in the northern region than in the south, greater in the plain area than in the mountain area, and largest in the northeast plain region. The impervious surface throughout the study area had characteristic expansion. This expansion

not only reflected an increase in land traffic, but also reflected the expansion of cities, among which impervious surface in the Changzhutan urban agglomerate in the northeast plain area experienced rapid expansion. Change in farmland in the mountain areas was more moderate than in the plain areas. In addition, large areas of wetlands in the northern part of the study area were converted into farmland.

Table 4. Conversion of land cover in Hunan Province for the period 2000–2010. Unit: km^2.

Land Cover	Woodland	Grassland	Wetland	Farmland	Impervious Surface	Bare Land	Transfer
Woodland	-	15.62	18.19	200.98	214.39	22.20	471.38
Grassland	4.56	-	0.02	1.93	0.51	0.01	7.03
Wetland	34.94	1.47	-	66.76	24.58	4.37	132.12
Farmland	183.87	5.57	70.02	-	445.74	17.68	722.88
Impervious surface	1.28	0.08	1.55	6.62	-	0.04	9.57
Bare land	12.77	0.33	5.35	18.55	7.52	-	44.52
Transferred into	237.42	23.07	95.13	294.84	692.74	44.30	-

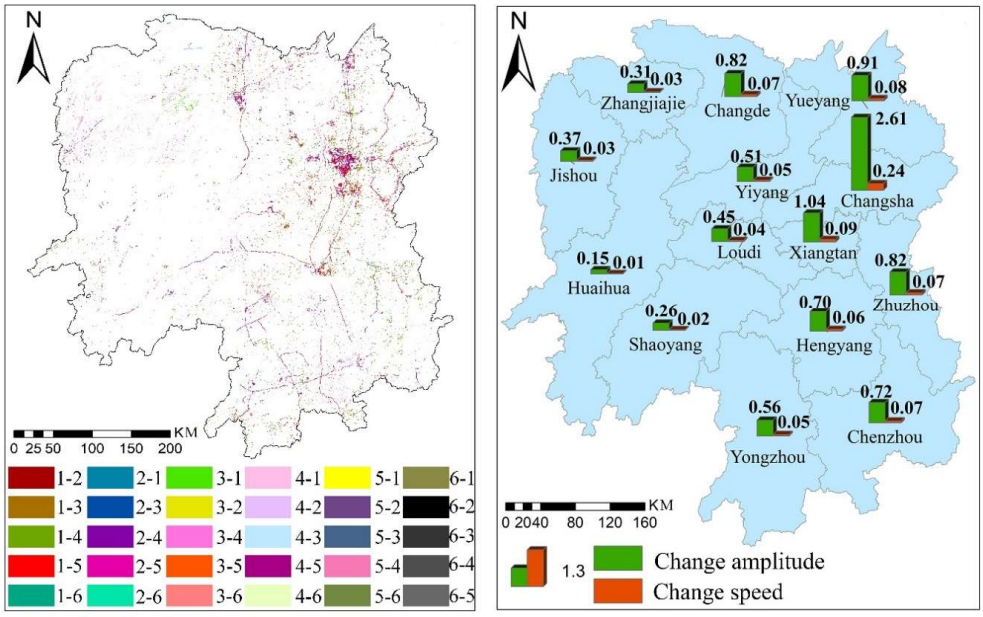

(**a**) (**b**)

Figure 6. Spatial distribution of (**a**) land cover conversion in Hunan Province in 2000–2010, and (**b**) the rate and range of land use change at prefectural level. Note: The numbers 1, 2, 3, 4, 5, and 6 represent woodland, grassland, wetland, farmland, impervious surface, and bare land, respectively. The combination of the two numbers is the conversion category of LUCC. For example, the code "1–2" denotes conversion of woodland to grassland.

4.3.3. Spatial Pattern at Prefecture Level

As shown in Figure 6b, a large spatial variation occurred in LUCCA and LUCCS in Hunan Province for 2000–2010. In general, the change in the east was greater than that in the west of Hunan Province. The Changzhutan urban agglomerate (including Chasha, Zhuzhou, and Xiangtan prefectures) and the surrounding Yueyang and Changde prefectures had the largest LUCCA and LUCCS. Changsha prefecture had the largest LUCCA and LUCCS in Hunan Province in 2000–2010, with values of 2.61 and 0.24, respectively. This was followed by Xiangtan Prefecture, with a LUCCA and LUCCS of 1.04 and 0.09, respectively. The third largest was Yueyang, with a LUCCA of 0.91 and LUCCS of 0.08. Zhuzhou ranked fourth with a LUCCA of 0.82 and LUCCS of 0.07. The LUCCA and LUCCS in Changede were 0.82 and 0.07, respectively, ranking fifth. There were diminishing

ranks of LUCCA and LUCCS for Chenzhou, Hengyang, Yongzhou, Yiyang, Loudi, Jishou, Zhangjiajie, Shaoyang, and Huaihua.

As shown in Figure 7, the highest transformation of LUCC was for impervious surface, by converting farmland into impervious surface (158.24 km^2), followed by woodland conversion into impervious surface (74.18 km^2), then farmland conversion into farmland (42.75 km^2), farmland conversion into forest land, and bare land conversion into impervious surfaces. For Xiangtan Prefecture, the top five transformations from largest to smallest were woodland conversion into impervious surface (20.87 km^2), farmland into impervious surface (15.75 km^2), woodland into farmland (8.47 km^2), wetland into impervious surface (1.27 km^2), and farmland into woodland (1.24 km^2). For Zhuzhou Prefecture, the top five LUCC from largest to smallest were woodland conversion into impervious surface (34.25 km^2), woodland into farmland (22.41 km^2), farmland into impervious surface (15.77 km^2), farmland into bare land (5.67 km^2), and woodland into wetland (2.58 km^2). The 189.76 km^2 of arable land in the Changsha–Zhuzhou–Xiangtan urban agglomerate consisted of 129.30 km^2 forest land and 6.12 km^2 wetland.

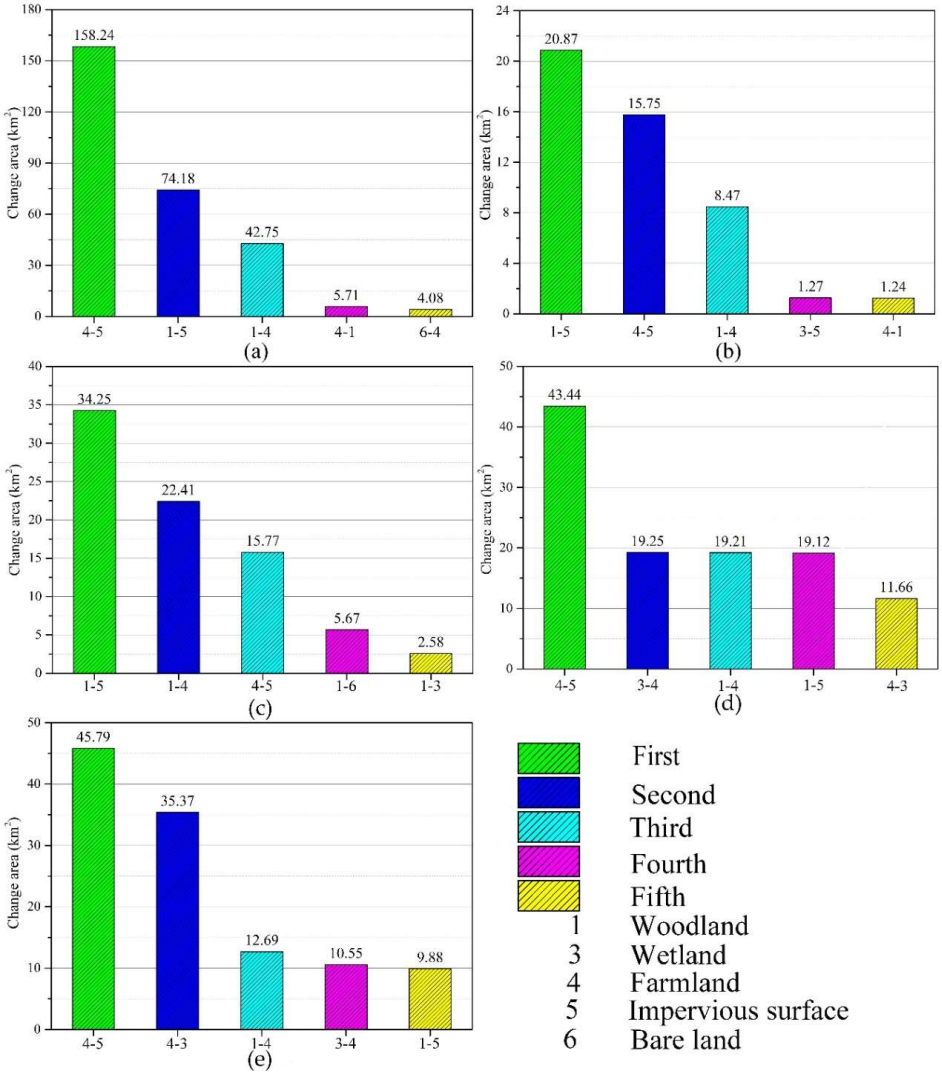

Figure 7. The top five land cover transformations in Changzhutan urban agglomerate, including (**a**) Changsha Prefecture; (**b**) Zhuzhou Prefecture; (**c**) Xiangtan Prefecture; and (**d**) the surrounding Yueyang and (**e**) Changde Prefecture. Note: The numbers 1, 3, 4, 5, and 6 represent woodland, wetland, farmland, impervious surface, and bare land, respectively. The combination of the two numbers is the conversion category of LUCC. For example, the code 4–5 denotes conversion of farmland to impervious surface.

The areas of 189.76 km^2 farmland, 129.30 km^2 woodland, and 6.12 km^2 wetland in the Changzhutan urban agglomerate were converted into impervious surface, most of which was from farmland in Changsha and Xiangtan and woodland in Zhuzhou. At the same time, 73.63 km^2 of woodland was converted into farmland in the Changzhutan urban agglomerate; with convertion areas in Changsha, Zhuzhou, and Xiangtan of 42.75 km^2, 22.41 km^2, and 8.47 km^2, respectively.

5. Discussion

5.1. Issues for OBIA

In this study, the results were smooth, compact, and largely consistent with actual conditions, without a "salt and pepper" phenomenon occurring in the results by using a traditional pixel-based method. The main reason for this result is that OBIA is based on a set of adjacent pixels with homogeneity, high physical significance, more available features, and boundary line matching with ground conditions [16,33]. More important, the accuracy of our results was relatively high. We attributed this high accuracy to the fact that OBIA not only uses spectral features of ground objects but also uses spatial features and textures, spatial structure features, shape, and other characteristics [1,10]. Thus, to a large extent, OBIA can overcome the negative effects of metameric substances with the same spectrum and a metameric spectrum with the same substance caused by using only spectrum features in traditional pixel-based methods to improve classification accuracy [11,12,22]. The OA and the Kappa coefficient of classification were 93.10% and 0.89, respectively. The OA and the Kappa coefficient of change detection were 86.42% and 84.32%, respectively. The accuracy of the results had high precision and a good effect. More important, the results showed that it was feasible to use medium-resolution HJ-CCD remote-sensing images and OBIA to monitor LUCC at a large scale. The method proposed in this study is based on medium-resolution remote-sensing images, but it can achieve a good monitoring effect. This provides important technical support for the rapid monitoring of regional land use change. Moreover, medium-resolution remote-sensing images are basically free of charge, so monitoring costs can be greatly reduced.

Our study proposed a large-scale monitoring LUCC method, which also has great reference value for the reconstruction of spatial information of land use in previous stages. Compared with previous object-oriented monitoring methods, the most important innovation of this method is the ability to transform the classification results of the current period (2010 year in this study) into the large sample that is required by the change region classification and to realize the full automation and high accuracy of the change region classification. This method can ensure that the accuracy of the land use classification results of the current stage is relatively high, because the land use map reconstructed in the past stages depends largely on the current map (in this study, the current stage is 2010 and the past stage is 2000). If the accuracy of the land use classification results for the current stage is not high, then it will directly affect the land use accuracy in the past stage and the classification results for the changing areas. This will further affect the monitoring accuracy of LUCC. The land use classification of the current stage has potential, and current data can be obtained for use as auxiliary information to obtain high-precision classification results, such as field samples. This is also why we first obtained the land use classification results in 2010, rather than in 2000, and then conducted the change monitoring.

The choice of an appropriate image segmentation scale is an important issue in large-scale LUCC monitoring using the OBIA technique [13,15,19]. For moderate-resolution images, the segmentation scale is too large, and many relatively small land use types and changing objects are submerged and cannot be extracted [34,35]. The oversize segmentation scale makes the computer burden heavier. Large-scale LUCC needs to subdivide the data in the research area into smaller data sets, thus increasing the workload [35]. Meanwhile, excessive segmentation may lead to additional broken patches on the image when monitoring results [34]. Some researchers have explored selection methods for an appropriate segmentation scale in small regions, but these methods are not mature enough to be used in large-scale LUCC monitoring [36]. Additionally, these methods are too complex,

which greatly increases the workload of large-scale LUCC monitoring, discounting the advantages of the rapid monitoring of remote sensing. In this study, we used the trial-and-error method to select the appropriate segmentation scale. The research results showed that the method is relatively simple and saves time when monitoring the LUCC on a large scale. Even if the most appropriate segmentation scale sometimes cannot be obtained, we can still choose a relatively small segmentation scale to ensure the accuracy of the results by weighing the impact of the segmentation scale. Of course, the trial-and-error method requires the operator to have good expert knowledge and visual interpretation ability and to be familiar with the land use status of the research area.

5.2. Driving Force of Land Use Pattern

The spatial distribution of land cover in Hunan Province was closely related to topography, government policy, and economic development [6,23,37]. There are series of mountains in the west, south, and north of Hunan Province, especially in the west region [27]. The western region of Hunan Province is a topographic transition zone between the first steppe (Xuefeng Mountain) and second steppe (Wushan Mountain). The south and east regions of Hunan Province include the Nanling and Luoxiao Mountains, respectively, and the northern region has Dabie and Tongbai Mountains [27]. The mountain areas had a poor natural environment, few people, and large areas of woodland. In the central and northern plains, especially in the Dongting Lake plain, large amounts of farmland and wetland existed [27]. Thus, this area represented an important food production base in China. With the rapid increase in population and economic development, farmland and impervious surfaces have become the main land cover types in plain areas. Government policy also has a great effect on land cover patterns in the study area, with Zhangjiajie in northwest China serving as a typical prefecture. Forest resources in Zhangjiajie are among China's and the world's most famous tourism prefectures, and the Wulingyuan scenic area is a world natural and cultural heritage site and world geological park. Many more areas are key national scenic spots [27]. The forest was strictly protected by the United Nations and China's government, and thus the forest land area was large [27]. Dongting Lake, the second largest freshwater lake in China, is in the north of Hunan Province, where strict protection measures have been implemented by the United Nations and the Chinese government as a key wetland reserve [38], thus providing a large wetland area.

5.3. Driving Force of LUCC Pattern

LUCC was the result of integrated action of the natural environment and human activity [2,5,39]. From 2000–2010, the government successively carried out major ecological projects, including returning farmland to woodland or grassland, natural forest protection, and returning farmland to lake [38,40]. Under the effect of these major ecological projects, the areas of farmland converted into woodland, grassland, and wetland in the study area in 2000–2010 were 183.87 km^2, 5.57 km^2, and 70.02 km^2, respectively, indicating some gains in ecological engineering construction. Rapid economic growth in the province, increasing resource exploitation, and accelerated urbanization for the period 2000–2010 also had the highest human disturbance in the region [27,40]. This disturbance has had a significant effect on land cover and also offset gains due to ecological engineering construction. Thus, the increases in woodland and wetland in 2000–2010 in the province were only 229.82 km^2 and 132.12 km^2, respectively. Woodland and wetland ecosystems have not improved.

Urbanization and economic development were the main causes of LUCC in the Changzhutan urban agglomerate and the surrounding areas in 2000–2010 [5,39,41]. From 2000–2010, the population density of the Changzhutan urban agglomerate increased rapidly [26,42]. The most obvious population growth was in the Changsha prefecture, with an average increase in population density of 20%, from 497 people/km^2 in 2000 to 595 people/km^2 in 2010 [26,43]. From 2000–2010, the average GDP of each prefecture in the region increased and LUCCA exceeded 100% [26]. The average GDP of Changsha increased from 5.7322 million RMB/km^2 in 2000 to 17.382 million RMB/km^2 in 2010, an increase of 2.03%. The average GDP of Zhuzhou increased by 5.367 million RMB/km^2 or 1.95% [26,43].

The average GDP of Xiangtan increased by 1.84% [26,42]. With such rapid urbanization and economic development, the LUCCA of the Changzhutan urban agglomerate was 1.61% and the LUCCA of Changsha, Zhuzhou, and Xiangtan were 2.61%, 1.04%, and 0.82%, respectively. In this process of change, 189.76 km^2 of farmland, 129.30 km^2 of woodland, and 6.12 km^2 of wetland was converted into impervious surface; Changsha and Xiangtan were mainly farmland and Zhuzhou was mainly encroached farmland. At the same time, 73.63 km^2 of woodland was converted into farmland in the Changzhutan urban agglomerate; the converted areas in Changsha, Zhuzhou, and Xiangtan totaled 42.75 km^2, 22.41 km^2, and 8.47 km^2, respectively. Changsha is the provincial capital of Hunan Province and it is also at the heart of Changzhutan urban agglomerate. Thus, LUCC in 2000–2010 in the study area was the largest in the agglomerate, with 232.42 km^2 of woodland and farmland converted into impervious surface, including 158.42 km^2 of farmland and 74.18 km^2 of woodland. The rapid urbanization and economic development in the Changzhutan urban agglomerate had a larger ripple effect on the surrounding Yueyang and Changde Prefectures. This caused the LUCC in these two prefectures to be the largest, followed by Changzhutan urban agglomerate.

5.4. Innovative Strategies

The method proposed in this study provides technical support for the monitoring of land-use change on a provincial or larger scale. On a large scale, it will take a great deal of staff power, material resources, and financial resources to manually investigate land use and its changes, and remote sensing is a cheap and fast method. Using high-resolution remote-sensing images is unlikely, however, because large areas of high-resolution images are expensive, which is difficult for decision makers to afford. The method we proposed is to use medium-resolution remote-sensing images, which solve this problem. Our proposed method can be used to investigate land use change and to provide basic information for decision-makers to determine the land use and its change situation in a region. This information also can be used to evaluate the effect of land use planning and policy implementation and to provide the basis for further adjustments in relevant policies.

Although the Chinese government's ecological project has achieved certain results, these achievements have been offset by the intensification of human activities, which eventually led to the unhealthy development of land use changes in Hunan Province from 2000 to 2010. This requires that we should further strengthen ecological protection and continue a series of ecological projects and also reduce the negative impact of human activities. To be specific, first, the speed of urban expansion needs to be controlled, especially in Changsha, Zhuzhou, and Xiangtan Prefectures. Second, the agricultural growth mode needs to change from an extensive growth mode to an intensive growth mode; that is, the growth of grain output mainly depends on the improvement of yield per unit area rather than simple continuous expansion of farmland area, especially in Changde and Yueyang Prefectures. In addition, the spatial difference of LUCC in Hunan Province from 2000 to 2010 is relatively large, which requires us to formulate different land use policies and land use spatial planning according to local conditions. In addition, the spatial difference of land use change needs to be monitored in real time by means of remote sensing and a geographic information system to provide rapid response for LUCC [37,44].

6. Conclusions

Based on the medium-resolution HJ-CCD remote sensing images, we used OBIA to monitor LUCC at provincial level. The conclusions from the study were as follows:

1. The OA of the land cover classification results for in Hunan Province in 2010 was 93.10%, with a Kappa coefficient of 0.89. The OA and the Kappa coefficient of detected change in the province were 86.42% and 0.84, respectively. This result showed high accuracy and a good effect, indicating the good performance of OBIA using HJ-CCD images. More important, the results showed that it was fully feasible to monitor large-scale LUCC using medium-resolution HJ-CCD remote-sensing images and OBIA;

2. Woodland in Hunan Province was mainly distributed in mountain areas in the west, south, and east. Wetland was distributed manly in the northern plains of the province and farmland was distributed mainly in central and northern plain areas and in mountain valleys. The largest impervious surface was in the Changzhutan urban agglomerate in the northeast plain area. The spatial distribution of land cover in Hunan Province was closely related to topography, government policy, and economic development;

3. From 2000–2010, the areas of farmland transformed into woodland, grassland, and wetland were, respectively, 183.87 km^2, 5.57 km^2, and 70.02 km^2, indicating some achievement by the ecological engineering construction drive. However, rapid economic growth, urbanization, and intense resource development offset the ecological engineering construction gains, and thus farmland and wetland areas decreased by 229.82 km^2 and 132.12 km^2, respectively, in Hunan Province during 2000–2010;

4. Spatial differences in LUCCA, LUCCS, and the transformation processes of LUCC at the prefectural level in Hunan Province were large. The Changzhutan urban agglomerate and the surrounding prefectures, including Changsha, Xiangtan, Zhuzhou, Yueyang, and Changde, had the largest LUCCA and LUCCS, where the dominant land cover conversion was from all of the other land use/cover into an impervious surface. For the period 2000–2010, 189.76 km^2 of farmland, 129.30 km^2 of woodland, and 6.12 km^2 of wetland were converted into impervious surfaces in the study area. This conversion was attributed mainly to the acceleration of urbanization and the rapid economic development in the above five prefectures.

Supplementary Materials: The following is available online at http://www.mdpi.com/2072-4292/10/12/2012/s1, Table S1: China's HJ-CDD images used in the study. Table S2: Appropriate segmentation scale of each small image piece.

Author Contributions: Conceptualization, K.L.; Methodology, K.L.; Software, B.L. and K.L.; Validation, B.L. and K.L.; Formal Analysis, K.L.; Investigation, B.L.; Resources, B.L.; Data Curation, K.L.; Writing-Original Draft Preparation, K.L.; Writing-Review & Editing, J.P.M.; Visualization, J.P.M.; Supervision, K.L.; Project Administration, K.L.; Funding Acquisition, K.L.

Funding: This research was funded by National Natural Science Foundation of China (Grant No. 41801200), the Foundation of Ministry of Culture and Tourism of China (Grant No. 18TAAG018), the Start-up Foundation for Introducing Talent of NUIST (Grant No. 2017r091) and College Student' Practice Innovation Training Program of NUIST (Grant No. 201810300096X).

Acknowledgments: We would like to thank the China Resources Satellite Application Center for providing some of the data. We also thank the anonymous reviewers and members of the editorial team for their comments and contributions.

Conflicts of Interest: The authors declare no conflict of interest.

References

1. Chen, Y.H.; Zhou, Y.N.; Ge, Y.; An, R.; Chen, Y. Enhancing Land Cover Mapping through Integration of Pixel-Based and Object-Based Classifications from Remotely Sensed Imagery. *Remote Sens.* **2018**, *10*, 77. [CrossRef]
2. Engelen, G.; White, R. Validating and Calibrating Integrated Cellular Automata Based Models of Land Use Change. In *The Dynamics of Complex Urban Systems*; Albeverio, S., Andrey, D., Giordano, P., Vancheri, A., Eds.; Physica-Verlag HD: Heidelberg, Germany, 2008; pp. 185–211.
3. Kok, J.L.D.; Overloop, S.; Engelen, G. Screening models for integrated environmental planning–A feasibility study for Flanders. *Futures* **2017**, *88*, 55–56. [CrossRef]
4. Soleimani, A.; Hosseini, S.M.; Bavani, A.R.M.; Jafari, M.; Francaviglia, R. Simulating soil organic carbon stock as affected by land cover change and climate change, Hyrcanian forests (northern Iran). *Sci. Total Environ.* **2017**, *599*, 1646–1657. [CrossRef] [PubMed]
5. White, R.; Uljee, I.; Engelen, G. Integrated modelling of population, employment and land-use change with a multiple activity-based variable grid cellular automaton. *Int. J. Remote Sens.* **2012**, *26*, 1256–1281. [CrossRef]
6. Batty, M.; Marshall, S. The origins of complexity theory in cities and planning. In *Complexity Theories of Cities Have Come of Age*; Springer: Berlin/Heidelberg, Germany, 2012; pp. 21–45.

7. Deng, X.Z.; Shi, Q.L.; Zhang, Q.; Shi, C.C.; Yin, F. Impacts of land use and land cover changes on surface energy and water balance in the Heihe River Basin of China, 2000–2010. *Phys. Chem. Earth* **2015**, *79*, 2–10. [CrossRef]
8. Cockx, K.; Van de Voorde, T.; Canters, F.; Poelmans, L.; Uljee, I.; Engelen, G.; de Jong, K.; Karssenberg, D.; Kwast, J. Incorporating land-use mapping uncertainty in remote sensing based calibration of land-use change. In Proceedings of the 8th International Symposium on Spatial Data Quality, Hong Kong, China, 30 May–1 June 2013; Volume XL-2/W1, pp. 7–12.
9. Jin, S.; Yang, L.; Zhu, Z.; Homer, C. A land cover change detection and classification protocol for updating Alaska NLCD 2001 to 2011. *Remote Sens. Environ.* **2017**, *195*, 44–55. [CrossRef]
10. Hao, M.; Shi, W.Z.; Deng, K.H.; Zhang, H.; He, P.F. An object-based change detection approach using uncertainty analysis for VHR images. *J. Sens.* **2016**, *2016*, 1–17. [CrossRef]
11. Chirici, G.; Mura, M.; Mcinerney, D.; Py, N.; Tomppo, E.O.; Waser, L.T.; Travaglini, D.; Mcroberts, R.E. A meta-analysis and review of the literature on the k-Nearest Neighbors technique for forestry applications that use remotely sensed data. *Remote Sens. Environ.* **2016**, *176*, 282–294. [CrossRef]
12. Hussain, M.; Chen, D.; Cheng, A.; Wei, H.; Stanley, D. Change detection from remotely sensed images: From pixel-based to object-based approaches. *ISPRS J. Photogramm. Remote Sens.* **2013**, *80*, 91–106. [CrossRef]
13. Baker, B.A.; Warner, T.A.; Conley, J.F.; McNeil, B.E. Does spatial resolution matter? A multi-scale comparison of object-based and pixel-based methods for detecting change associated with gas well drilling operations. *Int. J. Remote Sens.* **2013**, *34*, 1633–1651. [CrossRef]
14. Sen, S.; Zipper, C.E.; Wynne, R.H.; Donovan, P.F. Identifying Revegetated mines as disturbance/recovery trajectories using an Interannual Landsat Chronosequence. *Photogramm. Eng. Remote Sens.* **2012**, *78*, 223–235. [CrossRef]
15. Zhai, D.L.; Dong, J.W.; Cadisch, G.; Wang, M.C.; Kou, W.L.; Xu, J.C.; Xiao, X.M.; Abbas, S. Comparison of Pixel- and Object-Based Approaches in Phenology-Based Rubber Plantation Mapping in Fragmented Landscapes. *Remote Sens.* **2018**, *10*, 1–20. [CrossRef]
16. Blaschke, T.; Hay, G.J.; Kelly, M.; Lang, S.; Hofmann, P.; Addink, E.; Feitosa, R.Q.; Meer, F.V.D.; Werff, H.V.D.; Coillie, F.V. Geographic Object-Based Image Analysis â—Towards a new paradigm. *ISPRS J. Photogramm. Remote Sens.* **2014**, *87*, 180–191. [CrossRef] [PubMed]
17. Georganos, S.; Grippa, T.; Vanhuysse, S.; Lennert, M.; Shimoni, M.; Kalogirou, S.; Wolff, E. Less is more: Optimizing classification performance through feature selection in a very-high-resolution remote sensing object-based urban application. *GISci. Remote Sens.* **2018**, *55*, 221–242. [CrossRef]
18. Ma, L.; Li, M.C.; Ma, X.X.; Cheng, L.; Du, P.J.; Liu, Y.X. A review of supervised object-based land-cover image classification. *ISPRS J. Photogramm. Remote Sens.* **2017**, *130*, 277–293. [CrossRef]
19. Lu, L.; Tao, Y.; Di, L. Object-based plastic-mulched landcover extraction using integrated Sentinel-1 and Sentinel-2 data. *Remote Sens.* **2018**, *10*, 1820. [CrossRef]
20. Nemmaoui, A.; Aguilar, M.; Aguilar, F.; Novelli, A.; Lorca, A. Greenhouse crop identification from multi-temporal multi-sensor satellite imagery using object-based approach: a case study from Almería (Spain). *Remote Sens.* **2018**, *10*, 1751. [CrossRef]
21. Durieux, L.; Kropáček, J.; de Grandi, G.D.; Achard, F. Object-oriented and textural image classification of the Siberia GBFM radar mosaic combined with MERIS imagery for continental scale land cover mapping. *Int. J. Remote Sens.* **2007**, *28*, 4175–4182. [CrossRef]
22. Toure, S.; Stow, D.; Shih, H.C.; Coulter, L.; Weeks, J.; Engstrom, R.; Sandborn, A. An object-based temporal inversion approach to urban land use change analysis. *Remote Sens. Lett.* **2016**, *7*, 503–512. [CrossRef]
23. Geurs, K.; Hoen, A.; Engelen, G.; van Wee, B. 30 years of spatial planning and infrastructure policies in the Netherlands: A success? In Proceedings of the Bijdrage Colloquium Vervoersplanologisch Speurwerk, Antwerpen, Belgium, 20–21 November 2003; pp. 151–170.
24. Su, M.; Jiang, R.; Li, R.R. Investigating Low-Carbon Agriculture: Case Study of China's Henan Province. *Sustainability* **2017**, *9*, 2295. [CrossRef]
25. Peng, J.D.; Liao, Y.F.; Jiang, Y.H.; Zhang, J.M.; Qi, X.R. Development of the homogenized monthly precipitation series during 1910–2014 and its changes in Hunan Province, China. *J. Water Clim. Chang.* **2017**, *8*, 791–801. [CrossRef]
26. Bureau, C.S. *Hunan Statistical Yearbook*; China Statistics Press: Beijing, China, 2011.

27. Huang, H.X.; Luo, Y.P.; Yin, F.R.; Yi, M.; Liao, X.Y.; Hu, S.L.; Xing, H.L. Analysis on the driving forces of compositions and pattern changes of ecosystem in Hunan Province. *J. Hunan Univ. Sci. Technol.* **2015**, *30*, 61–67.
28. Wu, M.Q.; Zhang, X.Y.; Huang, W.J.; Niu, Z.; Wang, C.Y.; Li, W.; Hao, P.Y. Reconstruction of Daily 30 m Data from HJ CCD, GF-1 WFV, Landsat, and MODIS Data for Crop Monitoring. *Remote Sens.* **2015**, *7*, 16293–16314. [CrossRef]
29. Bernstein, L.S.; Jin, X.M.; Gregor, B.; Adler-Golden, S.M. Quick atmospheric correction code: Algorithm description and recent upgrades. *Opt. Eng.* **2012**, *51*, 111719–111724. [CrossRef]
30. Xian, G.; Homer, C.; Fry, J. Updating the 2001 National Land Cover Database land cover classification to 2006 by using Landsat imagery change detection methods. *Remote Sens. Environ.* **2009**, *113*, 1133–1147. [CrossRef]
31. Zhao, Y.S. *Principle and Method of Remote Sensing Application and Analysis*; Science Press of China: Beijing, China, 2012.
32. Liu, W.; Liu, J.; Kuang, W.; Jia, N. Examining the influence of the implementation of Major Function-oriented Zones on built-up area expansion in China. *J. Geogr. Sci.* **2017**, *27*, 643–660. [CrossRef]
33. Dronova, I. Object-Based Image Analysis in Wetland Research: A Review. *Remote Sens.* **2015**, *7*, 6380–6413. [CrossRef]
34. Drăguţ, L.; Csillik, O.; Eisank, C.; Tiede, D. Automated parameterisation for multi-scale image segmentation on multiple layers. *ISPRS J. Photogramm.* **2014**, *88*, 119–127. [CrossRef]
35. Schultz, B.; Immitzer, M.; Formaggio, A.; Sanches, I.; Luiz, A.; Atzberger, C. Self-guided segmentation and classification of multi-temporal Landsat 8 images for crop type mapping in southeastern Brazil. *Remote Sens.* **2015**, *7*, 14482–14508. [CrossRef]
36. Luo, K.; Li, R.D.; Chang, B.R.; Qiu, J.; Yi, F.J. Rearch progress in choosing objected-oriented optimal segmentation scale. *World Sci. Technol. Res. Dev.* **2013**, *35*, 75–79.
37. Woldesenbet, A. Land use land cover change detection by using remote sensing data in Akaki River Basin. *J. Food Agric. Environ.* **2016**, *1*, 153–176.
38. You, J.; Zhang, H.Q.; Chen, Y.F. Based on the GF-4 satellite image for the east dongting lake wetland vegetation type monitoring ability. *J. Anhui Agric. Sci.* **2018**, *3*, 33–39.
39. Gomes, E.; Banos, A.; Abrantes, P.; Rocha, J. Assessing the Effect of Spatial Proximity on Urban Growth. *Sustainability* **2018**, *10*, 1308. [CrossRef]
40. Jiankang, Z.; Jinxing, Z.; Huaiqing, Z.; Depeng, Y.; Ming, C.; Xiaorong, Z. Analysis on the driving force of the Returning Farmland to Lake Project and its impacts on wetland of West Dongting Lake. *For. Resour. Manag.* **2010**, *4*, 69–73.
41. Alzamili, H.; El-Mewafi, P.D.M.; Beshr, A.; Hadeal, M.; Ashraf, D.; Beshr, M. Monitoring urban growth and land use change detection with GIS and remote sensing techniques in Daqahlia governorate Egypt. *Int. J. Sustain. Built Environ.* **2015**, *6*, 117–124. [CrossRef]
42. Tang, F.H.; Chen, L.L. The evolution of regional differences of Changzhutan Urban Agglomeration since the 1990. *Geogr. Res.* **2011**, *30*, 94–102. [CrossRef]
43. Liao, L.; Qin, J. Ecologica security of wetland in Chang-Zhu-Tan urban agglomeration. *J. GeoInf. Sci.* **2016**, *18*, 1217–1226. [CrossRef]
44. Mallupattu, P.K.; Reddy, J.R.S. Analysis of Land Use/Land Cover Changes Using Remote Sensing Data and GIS at an Urban Area, Tirupati, India. *Sci. World J.* **2013**, *2013*, 1–6. [CrossRef] [PubMed]